An unaccounted pathway for rapid aging of atmospheric soot

Alexei F. Khalizov,[a,b]* Ella V. Ivanova,[b,§,#] Egor V. Demidov,[b#] Ali Hasani,[a] Jeffrey H. Curtis,[c] Nicole Riemer,[c] and Gennady Y. Gor[b]

[a] Department of Chemistry and Environmental Science, New Jersey Institute of Technology, Newark, New Jersey 07102, United States.

[b] Department of Chemical and Materials Engineering, New Jersey Institute of Technology, Newark, New Jersey 07102, United States.

[c] Department of Atmospheric Sciences, School of Earth, Society and the Environment, University of Illinois at Urbana-Champaign, Urbana, IL 61801, United States.

[§] Current address is Department of Chemical Environmental Engineering, University of California at Riverside, Riverside, CA 92521

[#] Equally contributed

* Corresponding author, khalizov@njit.edu

Abstract

Soot is a short-lived climate forcing agent whose warming potential varies significantly during its atmospheric lifetime. The particles of soot have a complex fractal morphology, but in atmospheric aerosol models they are commonly represented as spheres. We show that taking the fractal morphology into consideration significantly accelerates the rate of aging of soot aerosol in the atmosphere because concave surfaces in fractal particles promote rapid capillary condensation of trace gas chemicals produced from the photochemical oxidation of volatile organic compounds, even when vapors of such chemicals are subsaturated. Our results suggest that by capillary condensation alone these chemicals can transform hydrophobic soot particles into cloud condensation nuclei within a few hours. Additionally, capillary condensation induces compaction of fractal soot even at a moderately elevated relative humidity, changing its transport and optical properties. Representing an important mechanism of atmospheric aging, capillary condensation has a profound effect on the evolution of direct and indirect climate impacts of soot, at a higher rate than previously recognized, and hence it must be incorporated into atmospheric aerosol models to improve their predictive power.

As overshooting climate targets becomes a distinct possibility,[1] various scenarios are proposed for bringing the global temperature down quickly. Most scenarios rely on implementing carbon dioxide removal [2] or even invoke use of various geoengineering approaches.[3] Yet, curbing emissions of soot may offer the greatest potential for slowing down climate change because of significantly shorter lifetime of soot relative to carbon dioxide and other greenhouse gases.[4, 5] A product of incomplete combustion, soot is ubiquitous worldwide [5] and can be present in more than half of ambient particles in highly polluted atmospheric environments.[6, 7] Due to its strong light absorption and poor light scattering,[8, 9] soot is a major global warming agent, and exposure to soot negatively affects human health.[10] In the atmosphere, aging of soot through interactions with other trace chemicals significantly alters its composition and morphology.[11-13] As a result, soot atmospheric lifetime,[14, 15] its deposition in the human respiratory tract,[16] and its direct [4] and indirect climate forcing [17] become modified, making the knowledge of soot aging pathways paramount for accurate predictions of its impacts. Whereas the importance of rigorous treatment of particle morphology in predicting soot impacts has been clearly demonstrated,[18] the role of morphology in evaluating its aging rate has remained elusive.

Soot particles formed by fossil fuel combustion are lacey and hydrophobic,[19] as illustrated in Fig. 1a. The hydrophobic soot particles are not scavenged from the atmosphere as easily as other aerosols and show little morphological variability between dry and humid environments. However, after mixing with water-soluble chemicals during atmospheric aging, soot particles can take up water and undergo compaction, as demonstrated in laboratory studies using both individual trace gas chemicals [20, 21] and mixtures of condensable chemicals produced through oxidation of precursor compounds.[22-24] Field studies conducted in urban environments have closely associated the morphological compaction of soot particles with the extent of their aging,[25, 26] and the presence of a thick coating has become a criterion for switching from fractal to compact morphology when predicting the impacts of soot in aerosol models.[27] Thus, the observation of compact soot particles lacking visible coatings reported by a field study conducted in a remote marine free troposphere and supported by cloud chamber experiments was rather unexpected.[28, 29] This compaction was attributed to cloud processing, where soot particles underwent a cloud droplet activation-evaporation cycle. However, since bare soot particles cannot form cloud droplets at atmospherically relevant water supersaturations,[19] small amounts of sulfuric acid or water-soluble oxidized organics must have condensed on those particles during aging, making them cloud active.[22, 30]

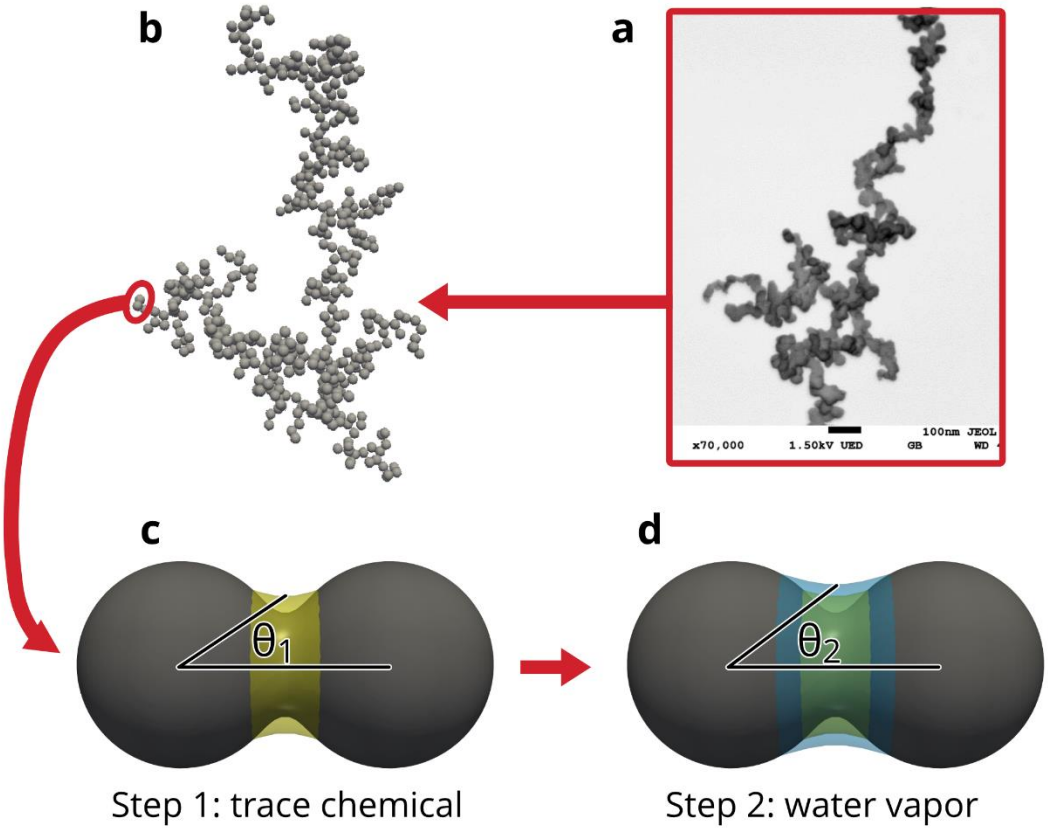

Fig. 1 | Morphological information about soot particles obtained by Scanning Electron Microscopy (**a**) is used to generate numerical soot particles as fractal aggregates of primary spheres (**b**). A fragment made of two spheres is used to represent an entire soot aggregate to model stepwise vapor condensation: **c**, capillary condensation of a trace chemical in the junction between the spheres and **d**, absorption of water vapor by concave aqueous meniscus. The amounts of condensate gained in steps 1 and 2 can be expressed via filling angles θ_1 and θ_2, respectively.

Aging of soot in a remote marine free troposphere would be a slow process in current aerosol models, as a significant vapor saturation is required to overcome the Kelvin effect and initiate the condensation of trace gas chemicals on bare soot particles, which are represented as spheres. On the contrary, our recent experiments have shown that in the case of real soot, even subsaturated vapors can condense promptly on fractal particles, resulting in minor but detectable compaction.[31] This has led us to hypothesize that concurrent capillary condensation of water-soluble trace chemicals and water vapor on fractal soot particles can result in their significant compaction and serve as a highly sensitive indicator of the transformation of initially hydrophobic soot to a hydrophilic state, and possibly to cloud condensation nuclei (CCN). To test this hypothesis, here we performed experiments where fractal soot particles were exposed to subsaturated vapors of several trace chemicals and then to progressively higher relative humidity (RH). To quantify the amounts of vapor

transferred to the particle phase, we modeled [32, 33] the step-by-step condensation of the trace chemical and water in concave menisci of the fractal soot particles, as shown in Fig. 1. We found that the depressed vapor pressure of the condensate above the menisci promoted rapid capillary condensation even under subsaturated conditions. To assess the role of capillary condensation in the aging of soot in the atmosphere, we extended our single-component model [32, 33] towards multi-component vapors and employed this new multi-component capillary condensation model (MCCCM) in conjunction with the particle-resolved PartMC-MOSAIC [34] aerosol model to explore a scenario representing the remote atmosphere.

Results and Discussion

Soot restructuring experiments. Subjecting size-classified soot aerosol (240 nm) to single-component vapors in a saturator reservoir partially filled with liquid or solid chemicals at room temperature produced no measurable increase in the particle mass. However, particle mobility diameter showed a small decrease (Fig. 2a, 5% RH). As reported previously,[31] such shrinkage of fractal soot after exposure to subsaturated vapors is indicative of capillary condensation, which places the condensate directly into junctions between the primary spheres, resulting in unbalanced forces that induce restructuring.[32, 35, 36] The absence of a measurable particle mass gain suggests that the amount of condensate in our experiments was less than 2-3%, the precision of our mass measurement. Such a mass gain corresponds to a coating thickness of $\sim$0.3 nm, if the condensate is distributed uniformly over the particle surface, or to a filling angle $\theta_1 = 35°$, if the condensate is placed entirely into junctions (Fig. 1c).

Despite the small amount of condensate, in most cases soot particles restructured when relative humidity was increased above its baseline value of 5%, and the response depended significantly on the coating material (Fig. 2a). The largest shrinkage was observed for soot particles treated with triethylene glycol (TEG) and its monobutyl ether (TEGMBE). Such particles restructured continuously with an increase in humidity, reaching maximum compaction at 85% RH, as also confirmed by Scanning Electron Microscopy (SEM) (Fig. 2d). Soot particles treated with ammonium nitrate (AN) and sulfuric acid (SA) also evolved continuously with an increase in humidity, but showed a lower ultimate shrinkage at RH 85%. A typical SEM image of such particles is presented in Fig. 2c. Notable is the absence of the deliquescence transition for AN, an effect previously reported for pure AN particles.[37] On the contrary, soot particles treated with glutaric acid (GA)

remained unchanged at RH below 70%, but showed a sharp shrinkage upon reaching the deliquescence point of GA, 83.5−85% RH.[38] Bare soot particles and soot particles treated with TDA showed no additional shrinkage during humidification because fresh soot is highly hydrophobic and TDA is immiscible with water. The difference in the extent of restructuring between different chemicals can be related to the condensate amount, which can be predicted by a numerical model, as described in the following section.

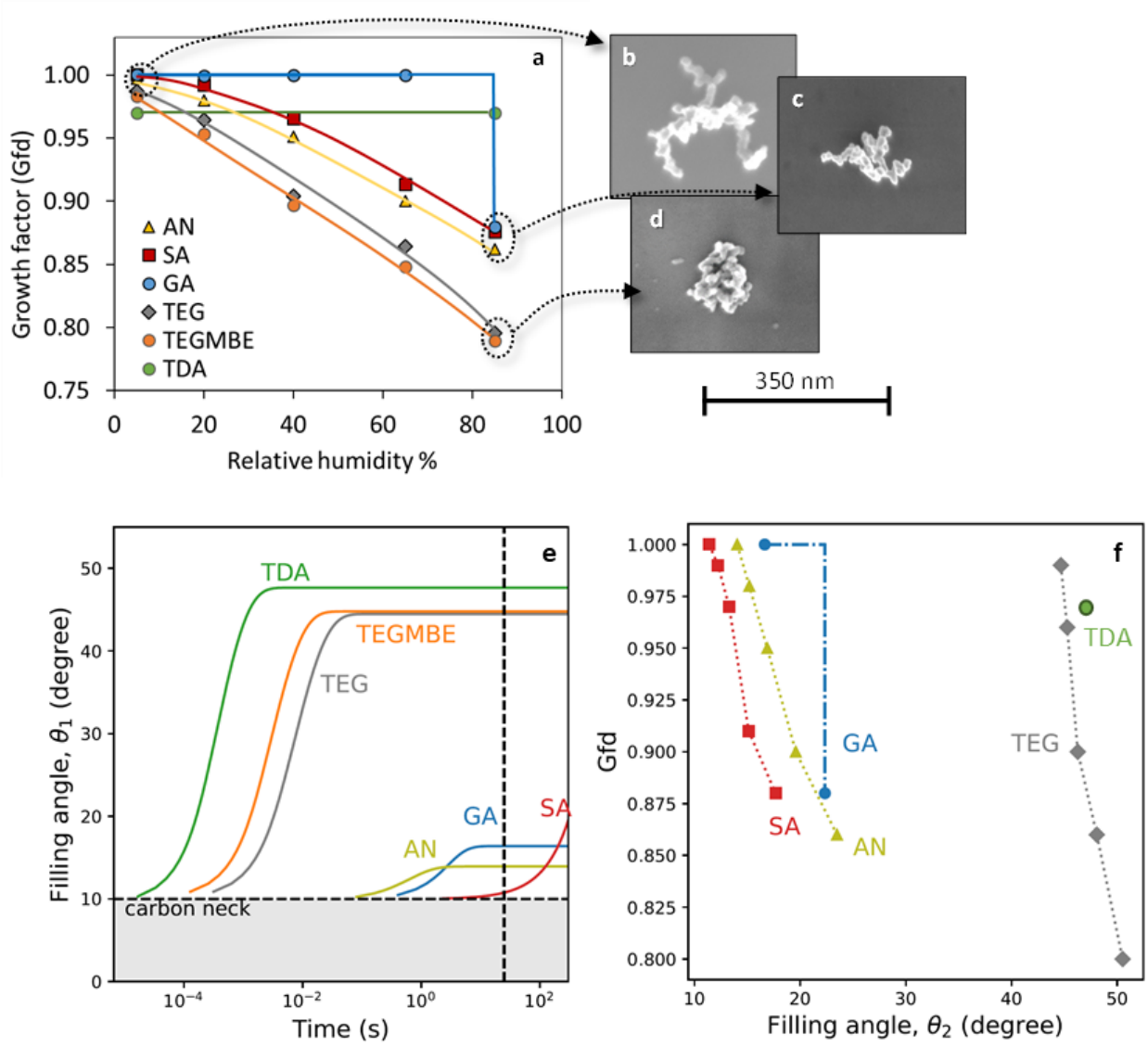

Fig. 2 | Morphological changes in soot particles exposed to subsaturated vapors of different trace gas chemicals and water obtained experimentally (**a**-**d**) and the amount of neat (**e**) and aqueous (**f**) condensate predicted by the model. Experiments include: **a**, particle growth factors and SEM images of **b**, fractal, **c**, partially restructured, and **d**, fully restructured soot aggregates. Model simulations of vapor condensation include: **e**, the filling angle (θ_1) of menisci made of different condensates at low humidity (the vertical dashed line marks the residence time of the soot aerosol in the saturator reservoir) and **f**, experimentally measured particle shrinkage (Gfd) as a function of the modeled filling angle (θ_2) of the humidified soot pre-

treated by different chemicals. TEGMBE is excluded in **f** due to lack of aqueous solution data. Initial mobility diameter of fractal soot particles is 240 nm, and the chemicals used are ammonium nitrate (AN), glutaric acid (GA), sulfuric acid (SA), tetradecane (TDE), triethylene glycol (TEG), and triethylene glycol monobutyl ether (TEGMBE). Gfd and several other parameters used to express changes in the particle size and morphology are defined in the Methods section.

Modeling of capillary condensation of vapors of individual chemicals and water. We used our recently developed capillary condensation model [32, 33] to predict the volume of condensate gained by fractal soot particles, as they traveled through the saturator. Fig. 2e shows the increase in volume, expressed as the filling angle θ_1 (see Fig. 1c-d for reference), for different chemicals. The zero time corresponds to the saturator entrance and the 10° initial filling angle is due to the carbon neck between primary spheres (Supplementary information, section 5). After entering the saturator, the aerosol flow became gradually saturated by the evaporating and diffusing chemical, reaching a vapor saturation $\nu = 0.9$ at the saturator exit. Despite identical vapor saturation for all chemicals, the model predicted vastly different condensate filling angles after a 25 s exposure: 48° for TDA, 45° for TEG and TEGMBE, 16° for GA, 14° for AN, and 11° for SA. One factor causing this spread was different wetting of the soot particle surface by different condensates. The second factor was related to the difference between vapor pressure above bulk material loaded in the saturator and vapor pressure above the condensate on particles. The latter was controlled by either the phase state or concentration of the chemical in the condensate, producing significantly different vapor saturations relative to particle phase, S (equation 4 in Methods, Supplementary sections 2 and 6). Despite the different saturation ratios, the filling angle of condensate reached a steady state value for all chemicals except for SA, corresponding to an equilibrium between the meniscus and surrounding vapor. The equilibrium was never achieved for SA because its vapor was highly supersaturated relative to particles ($S = 11.9$) due to a significant stabilization of the SA condensate by hydration even at the residual 5% RH (Supplementary section 6). The high supersaturation of SA vapor produced an exponential increase in the filling angle with exposure time, but the total amount of condensate gained by the particles upon exiting the reservoir was limited by the low SA saturation vapor pressure. Overall, mass fractions of condensed chemicals predicted by our model were 0.1–3.7%, ranging from well below (SA) to slightly above (TDA) experimentally detectable mass gain. Such small amounts, when placed in the junctions, created sufficiently strong capillary forces to initiate small but measurable restructuring of the soot aggregates. Indeed, comparing θ_1 at the saturator exit predicted by the model (Fig. 2e) against the extent of restructuring at the lowest

humidity measured in the experiments (Fig. 2a) shows a clear trend, where a higher θ_1 corresponds to a more significant decrease in the particle growth factor by diameter, Gfd. This observation is in agreement with previous studies performed using significantly larger amounts of single-component condensates.[20, 21, 39] In the following, we describe the increase in the filling angle by capillary condensation of water when these hydrophilic soot aggregates were exposed to progressively higher RH.

Most chemicals in our study can absorb water vapor, increasing in volume by a factor of $1.6 - 4.1$ at 85% RH (Supplementary Table 8). For most atmospheric particles this hygroscopic growth is partially suppressed by the positive curvature from the Kelvin effect, but in fractal soot the curvature is negative in the gaps between primary spheres, promoting capillary condensation of water, and resulting in a higher growth factor by volume, Gfv. To compute the equilibrium fraction of absorbed water in menisci, we used an iterative procedure (Supplementary section 7), similar to the previous work.[40] The predicted dependence of the humidified filling angle θ_2 on RH (Supplementary Fig. 6) shows an increase in the meniscus volume, corresponding to an estimated Gfv of 19.0, 9.3, 3.5, and 2.4 for SA, AN, GA, and TEG, respectively. These values are well in excess of the bulk Gfv values, pointing to the enhancement of water vapor absorption on hydrophilic soot aggregates by the capillary effect.

By combining the experimental Gfd with the calculated humidified θ_2, we relate the degree of restructuring to the amount of aqueous condensate in Fig. 2f. Like in Fig. 2a, the points form two clusters: (1) TEG and (2) GA, AN, and SA. Here TEG shows the largest filling angle and the most significant decrease in Gfd. Despite its lowest hygroscopicity, TEG produced the most condensate under dry and humid conditions because of the relatively low contact angles of its neat liquid and aqueous solution. GA experienced a deliquescence transition at 85% RH, absorbing a larger than TEG amount of water, but producing less restructuring because at low RH it condensed in a smaller amount due to both a higher contact angle (Supplementary Table 2) and a lower vapor saturation (Supplementary section 6). In the case of AN, the small initial volume increased significantly after humidification due the high hygroscopicity of this chemical, resulting in θ_2 and Gfd comparable to those of GA. The filling angle of SA increased significantly during humidification because of its high hygroscopicity. Despite the small amount, SA caused comparable to GA restructuring upon humidification that may be related to the higher surface tension of SA, resulting in stronger capillary

forces.[35, 41] Furthermore, SA condensed not only in the junctions but also over the entire particle surface.[32, 33] Hence, after humidification some of the aqueous SA condensate could be transported into the junctions, resulting in a larger filling angle than that predicted by our model. During this transport, the high contact angle of aqueous SA could have induced dynamic effects related to the condensate contact line pinning,[42] producing larger momentary forces, which enhanced restructuring.

Capillary condensation on fractal soot in the atmosphere. Under realistic atmospheric conditions, soot particles are exposed to multiple condensing chemicals that are present at significantly lower concentrations than in our laboratory experiments. To assess the role of capillary condensation on soot in the atmosphere, we extended our model towards multi-component vapors (Supplementary section 8). We then used this multi-component capillary condensation model (MCCCM) in conjunction with the particle-resolved PartMC-MOSAIC aerosol model [34] to explore relevant atmospheric scenarios. Here we illustrate our findings using a remote atmosphere scenario, because in a polluted urban atmosphere the condensation of highly supersaturated sulfuric acid can mask the contribution from capillary condensation of subsaturated organic vapors.

In this remote atmosphere scenario (Fig. 3a), soot emitted in an urban area (e.g., Durham, NC) during the night travels above a forested land (e.g., Duke Forest, NC), undergoing aging by the oxidation products of biogenic monoterpenes represented in PartMC-MOSAIC by α-pinene and limonene. Anthropogenic hydrocarbons are present in lower concentrations and their oxidation products contribute insignificantly. These organic oxidation products are hydrophilic but not hygroscopic, and hence do not absorb water at RH < 100%. Upon sunrise around 7 am, the gaseous oxidation products begin to build up, peaking in the late afternoon and then decreasing in concentration (Fig. 3b) as a result of an interplay between their generation from precursor hydrocarbons (Supplementary Fig. 9d and 10a), partitioning to existing aerosol, and dilution due to the variation in boundary layer height (Supplementary Fig. 9c). The vapor saturation, S_{tot}, which is the sum of individual saturations of condensable species, lags behind the concentrations due to elevated daytime temperatures (Supplementary Fig. 9a). When no absorbing material is initially present on soot particles, the condition $S_{\mathrm{tot}} > 1$ is used as a threshold for the formation of organic condensate.[43] In the biogenic scenario, this condition is met during a relatively narrow period between 4:30 pm and 10:30 pm. Hence, spherical soot particles, as implemented in PartMC-MOSAIC, remain bare throughout the

morning and most of the afternoon (Fig. 3c). Their growth begins only around 4:30 pm, peaking at a condensate volume fraction of 0.12 just before midnight, when about 20% of these particles become CCN at an atmospherically relevant water supersaturation of 0.2% (Fig. 3d).

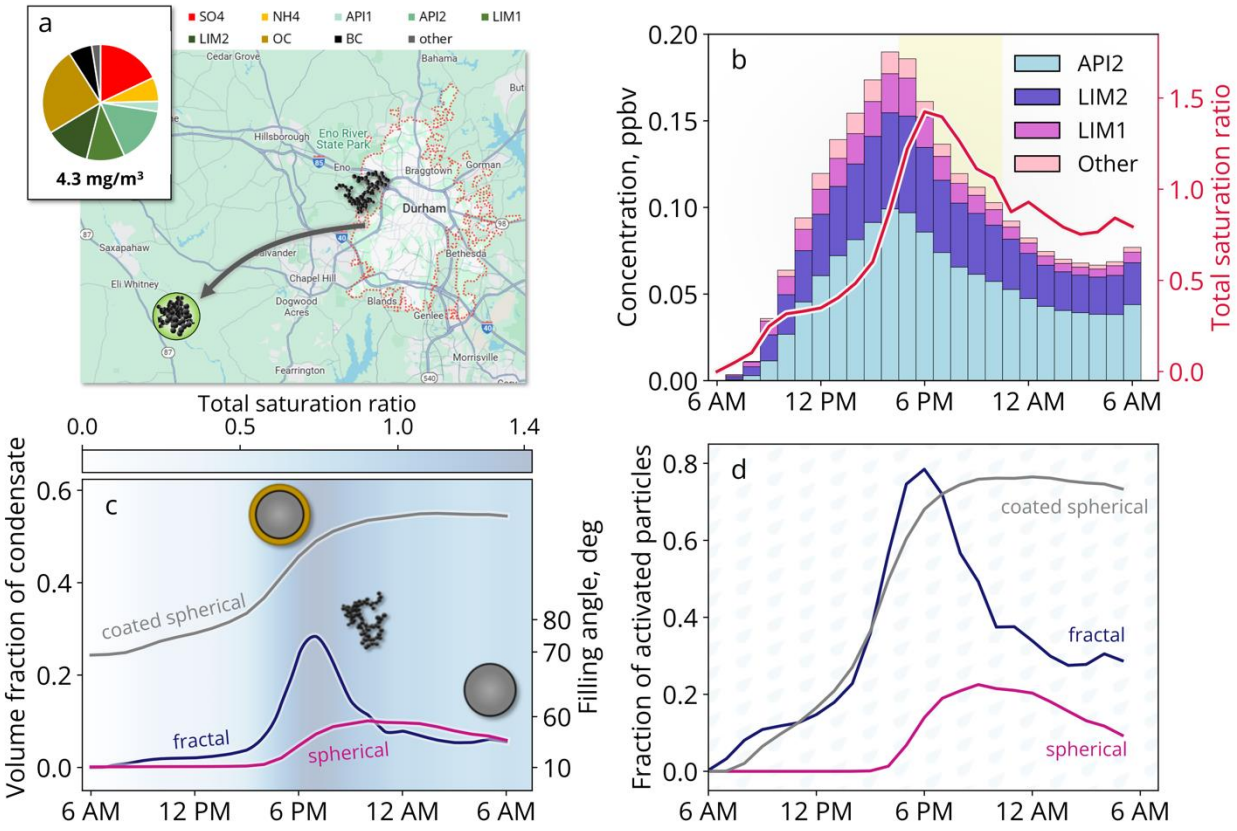

Fig. 3 | The conversion of hydrophobic atmospheric soot to cloud condensation nuclei predicted using fractal and spherical particle representations. **a**, An anthropogenic-biogenic interaction scenario used in the PartMC-MOSAIC simulation (map data ©2024 Google). The pie chart shows the average total aerosol composition in the early afternoon. API1 and API2 are produced from α-pinene; LIM1 and LIM2 are produced from limonene. **b**, Gas-phase concentrations of trace chemicals produced upon photochemical oxidation of anthropogenic and biogenic hydrocarbons, along with total vapor saturation, which is the sum of individual saturations of condensable species. The yellow band marks the time interval when the total saturation exceeded unity. **c**, Volume fractions of condensate modeled using three morphological representations of soot particles: fractal, spherical, and spherical coated with OC. For fractal soot particles, the filling angle of condensate is provided (see Fig. 1 for its definition). Background gradient reflects the evolution in the total vapor saturation of condensable vapors during the day. **d**, The fraction of soot particles becoming cloud condensation nuclei at a water supersaturation of 0.2%, using three different morphological representations.

On the contrary, as predicted by MCCCM, capillary condensation on fractal soot begins already at 7 am (Fig. 3c), and by 9 am there is sufficient amount of condensate to make nearly 10% of soot particles CCN-active (Fig. 3d). The prompt condensation on fractal soot at low S_{tot} is a result of the

vapor pressure depression from the negative meniscus curvature (Supplementary Fig. 10d), giving such fractal particles a significant advantage over spherical particles. The volume fraction of condensate closely follows S_{tot} and peaks at 0.34 around 7 pm, when nearly 80% of fractal soot particles become CCN. Although in later hours some of the condensate is lost by evaporation, a significant fraction of particles remain cloud active. Notably, when the filling angle reaches 45° at 4 pm (Fig. 3c), fractal aggregates are expected to begin restructuring (Fig. 2f), becoming significantly compacted by 7 pm when the filling angle reaches 80°. The partial evaporation of the condensate during late afternoon would convert these aggregates into highly compact globules.[31] Although described as solid spheres in aerosol models, such compact globules possess appreciable void space that can be treated as pores and hold significant amount of condensate.[44] If such atmospheric soot were sampled in the afternoon, it would be found to consist of soot particles that are compact, but lack visible coating, as has been reported earlier in field studies conducted at various locations.[29, 45, 46] Notably, the morphological and CCN behavior similar as predicted by our MCCCM model has been observed in chamber experiments with fractal soot aged by OH-initiated photochemical oxidation of monoethanolamine.[24] Intermediate volatility oxidation products of monoethanolamine underwent reversible capillary condensation, causing a partial collapse of soot aggregates at a condensate mass fraction of 17%. The CCN activity of such particles followed the amount of condensate, increasing initially and then decreasing when the condensate partially evaporated.[24] Another remarkable feature observed in our simulation is that after midnight, despite the lower average amount of condensate (Fig. 3c) fractal soot is more CCN active than spherical soot (Fig. 3d). This is because for fractal particles the fraction of condensate does not vary with the size of aggregates, whereas for spherical particles it decreases with increasing particle size, making larger spherical particles relatively less hygroscopic. Since cloud activation depends both on particle size and amount of water-soluble material, fractal soot produces more CCN.

The rapid processing of fractal soot by capillary condensation in a remote environment, as shown in our simulations, may alter soot properties and climate impacts faster than predicted in the atmospheric models using the spherical particle representation. Decreased size and increased hydrophilicity of such processed soot particles will shorten their atmospheric lifetime by accelerating coagulation and scavenging. Water taken up into pores of hydrophilic soot aggregates by capillary condensation can freeze homogeneously at cirrus temperatures and subsequently grow into macroscopic ice crystals.[44] Soot particles acting as cloud condensation and ice nuclei can change the

structure and radiative effects of clouds, e.g., leading to a reduction in low-level clouds and an increase in high-altitude cirrus cloud thickness, exacerbating the global mean surface warming.[17] When embedded inside cloud droplets, soot particles show a significant amplification in light absorption, nearly by an order of magnitude.[47, 48] After droplet evaporation, thinly coated compact soot particles would have a comparable light absorption but a 50% larger light scattering than the original fractal aggregates,[49] resulting in a larger single scattering albedo.[29]

We tested if it is possible to reproduce the aging rate of fractal soot by using spherical particles pre-coated with non-volatile and water-insoluble organic material (OC) to promote partitioning in lieu of capillary condensation. Fig. 3c shows that at a 0.25 volume fraction of OC, spherical soot particles gain condensate at a comparable rate as fractal particles because OC absorbs subsaturated vapors. Accordingly, such mixed particles show comparable to fractal particles CCN activity (Fig. 3d). However, the optical properties of such fresh OC-containing particles differ significantly from bare soot, exhibiting higher light scattering and absorption, by 45% and 12%, respectively. Hence, an improvement in the treatment of indirect effect of soot comes at the expense of a biased treatment of its direct effect. Additionally, when vapor saturation drops at night, the condensate does not evaporate off such mixed particles like in the case of fractal soot (Fig. 3c), making it impossible to explain observations of uncoated compact aggregates reported in field measurements. Hence, capillary condensation must be incorporated into atmospheric aerosol models explicitly to improve their predictive power.

Online content

Any methods, additional references, Nature Portfolio reporting summaries, source data, extended data, supplementary information, acknowledgements, peer review information; details of author contributions and 1competing interests; and statements of data and code availability are available online.

References

1. Reversing climate overshoot. *Nature Geoscience* 2023, **16**(6)**:** 467-467.

2. Fuhrman J, Bergero C, Weber M, Monteith S, Wang FM, Clarens AF, *et al*. Diverse carbon dioxide removal approaches could reduce impacts on the energy–water–land system. *Nature Climate Change* 2023, **13**(4)**:** 341-350.

3. Morrison TH, Adger WN, Agrawal A, Brown K, Hornsey MJ, Hughes TP, *et al.* Radical interventions for climate-impacted systems. *Nature Climate Change* 2022, **12**(12)**:** 1100-1106.

4. Ramana MV, Ramanathan V, Feng Y, Yoon SC, Kim SW, Carmichael GR, *et al.* Warming influenced by the ratio of black carbon to sulphate and the black-carbon source. *Nature Geosci* 2010, **3**(8)**:** 542-545.

5. Bond TC, Doherty SJ, Fahey DW, Forster PM, Berntsen T, DeAngelo BJ, *et al.* Bounding the role of black carbon in the climate system: A scientific assessment. *J Geophys Res* 2013, **118**(11)**:** 5380-5552.

6. Ma Y, Li S, Zheng J, Khalizov A, Wang X, Wang Z, *et al.* Size-resolved measurements of mixing state and cloud-nucleating ability of aerosols in Nanjing, China. *J Geophys Res, Atmos* 2017, **122**(17)**:** 9430-9450.

7. Zhou Q, Cheng C, Yang S, Yuan M, Meng J, Gong H, *et al.* Enhanced mixing state of black carbon with nitrate in single particles during haze periods in Zhengzhou, China. *Journal of Environmental Sciences* 2022, **111:** 185-196.

8. Bond TC, Bergstrom RW. Light absorption by carbonaceous particles: An investigative review. *Aerosol Science and Technology* 2006, **40**(1)**:** 27-67.

9. Ramanathan V, Carmichael G. Global and regional climate changes due to black carbon. *Nature Geosci* 2008, **1**(4)**:** 221-227.

10. Brugge D, Durant JL, Rioux C. Near-highway pollutants in motor vehicle exhaust: A review of epidemiologic evidence of cardiac and pulmonary health risks. *Environmental Health* 2007, **6**(1)**:** 23.

11. China S, Mazzoleni C, Gorkowski K, Aiken AC, Dubey MK. Morphology and mixing state of individual freshly emitted wildfire carbonaceous particles. *Nat Commun* 2013, **4**(1)**:** 2122.

12. Schwarz JP, Gao RS, Spackman JR, Watts LA, Thomson DS, Fahey DW, *et al.* Measurement of the mixing state, mass, and optical size of individual black carbon particles in urban and biomass burning emissions. *Geophys Res Letts* 2008, **35:** L13810.

13. Moteki N, Kondo Y, Miyazaki Y, Takegawa N, Komazaki Y, Kurata G, *et al.* Evolution of mixing state of black carbon particles: Aircraft measurements over the western Pacific in March 2004. *Geophys Res Letts* 2007, **34:** L11803.

14. Taylor JW, Allan JD, Allen G, Coe H, Williams PI, Flynn MJ, *et al.* Size-dependent wet removal of black carbon in Canadian biomass burning plumes. *Atmos Chem Phys* 2014, **14**(24)**:** 13755-13771.

15. Stier P, Seinfeld JH, Kinne S, Feichter J, Boucher O. Impact of nonabsorbing anthropogenic aerosols on clear-sky atmospheric absorption. *J Geophys Res, Atmos* 2006, **111:** D18201.

16. Broday DM, Rosenzweig R. Deposition of fractal-like soot aggregates in the human respiratory tract. *J Aerosol Sci* 2011, **42**(6)**:** 372-386.

17. Lohmann U, Friebel F, Kanji ZA, Mahrt F, Mensah AA, Neubauer D. Future warming exacerbated by aged-soot effect on cloud formation. *Nature Geoscience* 2020, **13**(10)**:** 674-680.

18. Romshoo B, Müller T, Ahlawat A, Wiedensohler A, Haneef MV, Imran M, *et al.* Significant contribution of fractal morphology to aerosol light absorption in polluted environments dominated by black carbon (BC). *npj Climate and Atmospheric Science* 2024, **7**(1)**:** 87.

19. Ma X, Zangmeister CD, Gigault J, Mulholland GW, Zachariah MR. Soot aggregate restructuring during water processing. *J Aerosol Sci* 2013, **66**(0)**:** 209-219.

20. Xue H, Khalizov AF, Wang L, Zheng J, Zhang R. Effects of Coating of Dicarboxylic Acids on the Mass-Mobility Relationship of Soot Particles. *Environ Sci Technol* 2009, **43**(8)**:** 2787-2792.

21. Khalizov AF, Zhang R, Zhang D, Xue H, Pagels J, McMurry PH. Formation of highly hygroscopic soot aerosols upon internal mixing with sulfuric acid vapor. *J Geophys Res* 2009, **114:** D05208.

22. Ma Y, Brooks SD, Vidaurre G, Khalizov AF, Wang L, Zhang R. Rapid modification of cloud-nucleating ability of aerosols by biogenic emissions. *Geophys Res Letts* 2013, **40:** 6293–6297.

23. Leung KK, Schnitzler EG, Jäger W, Olfert JS. Relative Humidity Dependence of Soot Aggregate Restructuring Induced by Secondary Organic Aerosol: Effects of Water on Coating Viscosity and Surface Tension. *Environmental Science & Technology Letters* 2017, **4**(9)**:** 386-390.

24. Chen C, Enekwizu OY, Ma X, Jiang Y, Khalizov AF, Zheng J, *et al.* Effect of organic coatings derived from the OH-initiated oxidation of amines on soot morphology and cloud activation. *Atmos Res* 2020, **239:** 104905.

25. Moffet RC, O'Brien RE, Alpert PA, Kelly ST, Pham DQ, Gilles MK, *et al.* Morphology and mixing of black carbon particles collected in central California during the CARES field study. *Atmos Chem Phys* 2016, **16**(22)**:** 14515-14525.

26. Xu L, Fukushima S, Sobanska S, Murata K, Naganuma A, Liu L, *et al.* Tracing the evolution of morphology and mixing state of soot particles along with the movement of an Asian dust storm. *Atmospheric Chemistry and Physics* 2020, **20**(22)**:** 14321-14332.

27. Kajino M, Kondo Y. EMTACS: Development and regional-scale simulation of a size, chemical, mixing type, and soot shape resolved atmospheric particle model. *J Geophys Res* 2011, **116:** D02303.

28. China S, Scarnato B, Owen RC, Zhang B, Ampadu MT, Kumar S, *et al.* Morphology and mixing state of aged soot particles at a remote marine free troposphere site: Implications for optical properties. *Geophys Res Letts* 2015, **42**(4)**:** 2014GL062404.

29. Bhandari J, China S, Chandrakar KK, Kinney G, Cantrell W, Shaw RA, *et al.* Extensive Soot Compaction by Cloud Processing from Laboratory and Field Observations. *Scientific Reports* 2019, **9**(1)**:** 11824.

30. Zhang R, Khalizov AF, Pagels J, Zhang D, Xue H, McMurry PH. Variability in morphology, hygroscopicity, and optical properties of soot aerosols during atmospheric processing. *Proc Natl Acad Sci USA* 2008, **105**(30)**:** 10291-10296.

31. Enekwizu OY, Hasani A, Khalizov AF. Vapor Condensation and Coating Evaporation Are Both Responsible for Soot Aggregate Restructuring. *Environ Sci Technol* 2021, **55**(13)**:** 8622-8630.

32. Chen C, Enekwizu OY, Fan X, Dobrzanski CD, Ivanova EV, Ma Y, *et al.* Single Parameter for Predicting the Morphology of Atmospheric Black Carbon. *Environ Sci Technol* 2018, **52**(24)**:** 14169-14179.

33. Ivanova EV, Khalizov AF, Gor GY. Kinetic model for competitive condensation of vapor between concave and convex surfaces in a soot aggregate. *Aerosol Science and Technology* 2020, **55**(3)**:** 1-19.

34. Riemer N, West M, Zaveri RA, Easter RC. Simulating the evolution of soot mixing state with a particle-resolved aerosol model. *J Geophys Res* 2009, **114:** D09202.

35. Kütz S, Schmidt-Ott A. Characterization of agglomerates by condensation-induced restructuring. *Journal of Aerosol Science* 1992, **23**(Supplement 1)**:** 357-360.

36. Demidov EV, Gor GY, Khalizov AF. Discrete element method model of soot aggregates. *Physical Review E* 2024, **110**(5)**:** 054902.

37. Jing B, Wang Z, Tan F, Guo Y, Tong S, Wang W, *et al.* Hygroscopic behavior of atmospheric aerosols containing nitrate salts and water-soluble organic acids. *Atmos Chem Phys* 2018, **18**(7)**:** 5115-5127.

38. Peng C, Chan MN, Chan CK. The hygroscopic properties of dicarboxylic and multifunctional acids: Measurements and UNIFAC predictions. *Environ Sci Technol* 2001, **35**(22)**:** 4495-4501.

39. Yuan C, Zheng J, Ma Y, Jiang Y, Li Y, Wang Z. Significant restructuring and light absorption enhancement of black carbon particles by ammonium nitrate coating. *Environmental Pollution* 2020, **262:** 114172.

40. Xie JY, Marlow WH. Water vapor pressure over complex particles .1. Sulfuric acid solution effect. *Aerosol Sci Technol* 1997, **27**(5)**:** 591-603.

41. Schnitzler EG, Gac JM, Jäger W. Coating surface tension dependence of soot aggregate restructuring. *J Aerosol Sci* 2017, **106:** 43-55.

42. Corbin JC, Modini RL, Gysel-Beer M. Mechanisms of soot-aggregate restructuring and compaction. *Aerosol Science and Technology* 2022, **57**(2)**:** 89-111.

43. Bowman FM, Odum JR, Seinfeld JH, Pandis SN. Mathematical model for gas-particle partitioning of secondary organic aerosols. *Atmospheric Environment* 1997, **31**(23)**:** 3921-3931.

44. Marcolli C, Mahrt F, Kärcher B. Soot PCF: pore condensation and freezing framework for soot aggregates. *Atmos Chem Phys* 2021, **21**(10)**:** 7791-7843.

45. China S, Scarnato B, Owen RC, Zhang B, Ampadu MT, Kumar S, *et al.* Morphology and mixing state of aged soot particles at a remote marine free troposphere site: Implications for optical properties. *Geophys Res Letts* 2015, **42**(4)**:** 1243-1250.

46. Wang Y, Xu L, Zhang Z, Zhang J, Liu L, Zhang Y, *et al.* Variability in morphology of soot particles during non-cloud and in-cloud processes. *Atmospheric Environment* 2024, **326:** 120489.

47. Markel VA, Shalaev VM. Absorption of light by soot particles in micro-droplets of water. *Journal of Quantitative Spectroscopy and Radiative Transfer* 1999, **63**(2)**:** 321-339.

48. Mishchenko MI, Liu L, Cairns B, Mackowski DW. Optics of water cloud droplets mixed with black-carbon aerosols. *Optics Letters* 2014, **39**(9)**:** 2607-2610.

49. Demidov EV, Enekwizu OY, Hasani A, Qiu C, Khalizov AF. Differences and similarities in optical properties of coated fractal soot and its surrogates. *J Aerosol Sci* 2024, **180:** 106392.

Methods

Experiments were conducted using an aerosol system, where combustion soot was size classified and then exposed to vapors of trace gas chemicals and water. Changes in the particle mobility diameter and particle mass were measured before and after processing, and in some experiments soot particles were collected for scanning electron microscopy (SEM) analysis.[1-4] Detailed descriptions of the experimental system and methods are provided in Supplementary Information Section 1.

Changes in the particle morphology are reported as diameter growth factor, Gfd, calculated by Equation 1, where D_{p} is the mobility diameter of the processed (coated, humidified, or coated-humidified) particles and D_{i} is the initial diameter. The relative error in Gfd measurement was less than 1%. Changes in the particle mass are reported as mass growth factor Gfm (Equation 2) and mass fraction f_{m} (Equation 3), where m_{i} is the initial particle mass and m_{p} is the particle mass after processing. The relative error in f_{m} was about 3%.

$$\mathrm{Gfd} = D_{\mathrm{p}}/D_{\mathrm{i}} \quad (1)$$

$$\mathrm{Gfm} = m_{\mathrm{p}}/m_{\mathrm{i}} \quad (2)$$

$$f_{\mathrm{m}} = 1 - 1/\mathrm{Gfm} \quad (3)$$

A simulation of laboratory experiments on the condensation of individual chemicals and water on soot aggregates was performed using a two-step approach. In the first step (Supplementary Information section 5), the condensation of a pure chemical was considered using a kinetic model that accounted for the convex surface of primary spheres and concave surface of meniscus in junctions between the spheres.[4, 5] The vapor pressure of the condensate is elevated above the convex surface and depressed above the concave surface due to the Kelvin effect associated with the positive and negative curvature, respectively. Due to the depressed saturation pressure above concave surfaces, condensation can occur even in subsaturated vapor ($S < 1$),

$$S = \frac{p_{\mathrm{gas}}}{p_{\mathrm{sat,p}}} \quad (4)$$

where p_{gas} is the unperturbed partial pressure of vapor far from the particle, $p_{\mathrm{sat,p}}$ is the saturation vapor pressure above the condensate on particles, and S is the vapor saturation. Irrespective of condensate location, its amount in the junction can be expressed via the filling angle θ_1 (Fig. 1c). In the second step, a thermodynamic model, described in Supplementary Information section 7, was used to calculate the amount of water taken by the water-soluble condensate located in the concave junction to produce an aqueous meniscus, which is in equilibrium with water vapor at 5–85% RH. The resulting amount of aqueous condensate is expressed as the filling angle θ_2 (Figure 1d). The relative increase in the volume of condensate is expressed as growth factor by volume

$$\mathrm{Gfv} = V_{\mathrm{RH}}/V_{\mathrm{RH=5\%}}, \quad (5)$$

where V_{RH} and $V_{\mathrm{RH=5\%}}$ are condensate volumes at a specific RH and 5% RH.

To assess the role of capillary condensation in the soot aging in the atmosphere, our condensation model was extended to account for multiple vapors and multi-component condensate. The resulting multi-component capillary condensation model (MCCCM) was used in conjunction with the particle-resolved PartMC-MOSAIC aerosol model[6] to explore relevant atmospheric scenarios, as described in Supplementary Information section 8. Cloud activation by aged soot particles was evaluated based on the particle volume fraction of condensate and particle volume equivalent diameter, using the κ-hygroscopicity framework.[7]

Data availability

Modeled and measured data produced in this study are available in Supplementary Information. Data obtained from publicly available sources are available from the references. Source data are provided with this paper.

Code availability

Codes for modeling the condensation of trace chemicals and water on soot aggregates are available from the authors upon request.

Acknowledgments

This study was supported by the National Science Foundation (AGS-2222104). SEM images were obtained at the Otto H. York Center for Environmental Engineering and Science at New Jersey Institute of Technology.

Author contributions

A.F.K – conceptualization, formal analysis, funding acquisition, investigation, methodology, project administration, resources, supervision, validation, visualization, writing – original draft, writing – review & editing. E.V.I. - formal analysis, investigation, methodology, software, visualization, writing – original draft. E.V.D. - formal analysis, investigation, methodology, software, validation, visualization, writing – original draft, writing – review & editing. A.H. - investigation, writing – original draft. J.H.C. – methodology, software. N.R. – conceptualization, validation. G.Y.G. – conceptualization, funding acquisition, methodology, supervision, writing – review & editing.

Competing interests

The authors declare no competing interests.

Additional information

Supplementary Information. The online version contains supplementary material.

Correspondence and requests for materials should be addressed to Alexei Khalizov.

References

1. Enekwizu OY, Hasani A, Khalizov AF. Vapor Condensation and Coating Evaporation Are Both Responsible for Soot Aggregate Restructuring. *Environ Sci Technol* 2021, **55**(13)**:** 8622-8630.

2. Chen C, Enekwizu O, Ma Y, Zakharov D, Khalizov A. The Impact of Sampling Medium and Environment on Particle Morphology. *Atmosphere* 2017, **8**(9)**:** 162.

3. Chen C, Fan X, Shaltout T, Qiu C, Ma Y, Goldman A, *et al.* An unexpected restructuring of combustion soot aggregates by subnanometer coatings of polycyclic aromatic hydrocarbons. *Geophys Res Letts* 2016, **43**(20)**:** 11,080-011,088.

4. Chen C, Enekwizu OY, Fan X, Dobrzanski CD, Ivanova EV, Ma Y, *et al.* Single Parameter for Predicting the Morphology of Atmospheric Black Carbon. *Environ Sci Technol* 2018, **52**(24)**:** 14169-14179.

5. Ivanova EV, Khalizov AF, Gor GY. Kinetic model for competitive condensation of vapor between concave and convex surfaces in a soot aggregate. *Aerosol Science and Technology* 2020, **55**(3)**:** 1-19.

6. Riemer N, West M, Zaveri RA, Easter RC. Simulating the evolution of soot mixing state with a particle-resolved aerosol model. *J Geophys Res* 2009, **114:** D09202.

7. Petters MD, Kreidenweis SM. A single parameter representation of hygroscopic growth and cloud condensation nucleus activity. *Atmos Chem Phys* 2007, **7**(8)**:** 1961-1971.